

Unusual phase boundary of the magnetic-field-tuned valence transition in $\text{CeOs}_4\text{Sb}_{12}$

K. Götze,¹ M. J. Pearce,¹ P. A. Goddard,¹ M. Jaime,² M. B. Maple,³ K. Sasmal,³
T. Yanagisawa,⁴ A. McCollam,⁵ T. Khouri,⁵ P.-C. Ho,⁶ and J. Singleton²

¹*Department of Physics, University of Warwick, Coventry CV4 7AL, UK.*

²*National High Magnetic Field Laboratory, Los Alamos National Laboratory, MS-E536, Los Alamos, New Mexico 87545, USA.*

³*Department of Physics, University of California, San Diego, La Jolla, CA 92093, USA.*

⁴*Department of Physics, Hokkaido University, Sapporo 060-0810, Japan*

⁵*High Field Magnet Laboratory (HFML-EMFL), Radboud University, Toernooiveld 7, 6525 ED, Nijmegen, The Netherlands*

⁶*Department of Physics, California State University, Fresno, CA 93740, USA.*

(Dated: December 21, 2024)

The phase diagram of the filled skutterudite $\text{CeOs}_4\text{Sb}_{12}$ has been mapped in fields H of up to 60 T and temperatures T down to 0.5 K using resistivity, magnetostriction, and MHz conductivity. The valence transition separating the semimetallic, low- H , low- T , \mathcal{L} phase from the metallic high- H , high- T \mathcal{H} phase exhibits a very unusual, wedge-shaped phase boundary, with a non-monotonic gradient alternating between positive and negative. This is quite different from the text-book “elliptical” phase boundary usually followed by valence transitions. Analysis of Shubnikov-de Haas oscillations within the \mathcal{H} phase reveals an effective mass that increases as H drops toward the $\mathcal{H} - \mathcal{L}$ phase boundary, suggesting proximity to a quantum-critical point. The associated magnetic fluctuations may be responsible for the anomalous H, T dependence of the valence transition at high H , whereas the low- H , high- T portion of the phase boundary may rather be associated with the proximity of $\text{CeOs}_4\text{Sb}_{12}$ to a topological semimetal phase induced by uniaxial stress.

Valence transitions, in which f -electrons undergo a temperature and/or magnetic-field driven transformation from itinerant to quasi-localized, are associated with significant changes in material properties [1–3] and dramatic alterations to the Fermi surface [1, 4]. Perhaps the best-known is the $\gamma - \alpha$ transition in Ce and its alloys, which leads to a spectacular volume collapse of the sample [2, 3]. Valence transitions are also thought to be responsible for the onset of the “hidden order phase” of URu_2Si_2 , plus some of the phase boundaries of elemental Pu [5–7]. A key identifying feature of valence transitions has been the resulting *elliptical phase boundary*: the magnetic field H and temperature T points at which the valence transition occurs lie on a straight line when plotted as H^2 versus T^2 , with the slope determined by the g -factor alone [4].

By contrast, we show here that the valence transition in $\text{CeOs}_4\text{Sb}_{12}$, identified by its effect on the Fermi surface and material properties [1], does not follow the above textbook elliptical behavior. We performed MHz conductivity, magnetostriction and resistivity measurements on $\text{CeOs}_4\text{Sb}_{12}$, to map out the phase diagram shown in Fig 1. The valence transition separates the low- T , low- H , semimetallic \mathcal{L} phase and the high- T , high- H , metallic \mathcal{H} phase [1]; it is immediately obvious that it behaves very unconventionally, falling back to lower T as $H \rightarrow 0$ and lower H as $T \rightarrow 0$. We suggest that this unusual behavior is due to a sensitivity of the low-temperature groundstates of $\text{CeOs}_4\text{Sb}_{12}$ to quantum fluctuations, and to a proximity to a topological semimetallic phase.

$\text{CeOs}_4\text{Sb}_{12}$ is part of an interesting series of rare-earth-based filled skutterudites that includes the unconventional superconductor $\text{PrOs}_4\text{Sb}_{12}$ [12, 13] and

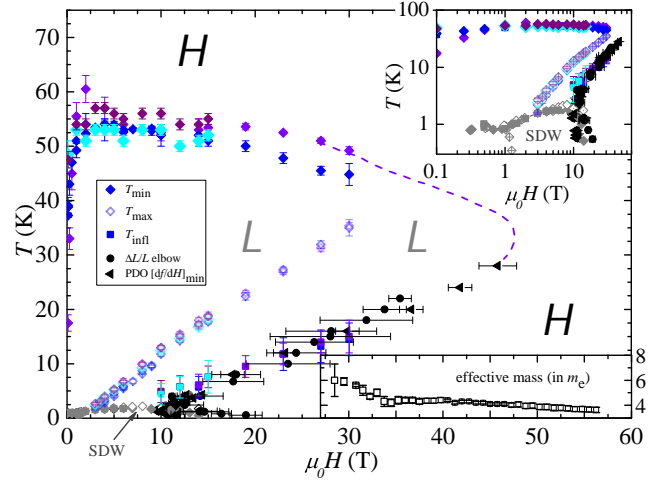


FIG. 1. T - H -phase diagram of $\text{CeOs}_4\text{Sb}_{12}$ derived from data in this work. Points are from resistivity (solid diamonds: T_{\min} , solid squares: T_{infl} , open diamonds: T_{\max} , different colors represent different samples), magnetostriction (solid circles) and MHz conductivity (solid triangles). Variables are defined in the text. The dotted line is a guide to the eye of a plausible completion of the \mathcal{L} - \mathcal{H} phase boundary. T_{\max} does not mark a phase transition but the onset of the return to metallic behavior at low T /high H . SDW phase boundary is taken from Refs. [8–11] (grey symbols). Upper inset: the phase diagram with logarithmic axes. Lower inset: H dependence of the effective mass derived from quantum oscillations.

ferromagnetic $\text{NdOs}_4\text{Sb}_{12}$ [1, 14]. While $\text{PrOs}_4\text{Sb}_{12}$ and $\text{NdOs}_4\text{Sb}_{12}$ possess similar Fermi surfaces comprising multiple pockets (but with different effective masses), $\text{CeOs}_4\text{Sb}_{12}$ exhibits a valence transition from the heavy-effective-mass (Sommerfeld coefficient $\gamma =$

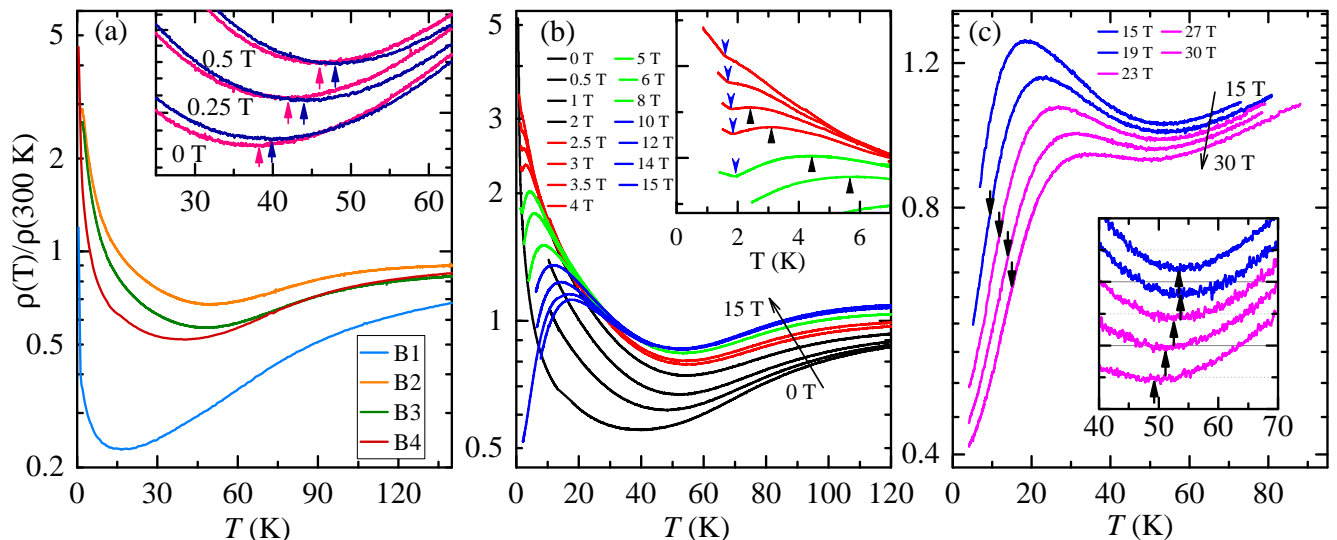


FIG. 2. (a) Resistivity ρ [normalized to $\rho(300\text{ K})$] of all four measured crystals (B1-B4) at $H = 0$ for $0.6 \leq T \leq 140$ K. Inset: hysteresis between warming and cooling (sample B4) for $\mu_0 H = 0, 0.25$ and 0.5 T. Arrows mark the minimum for warming (red) and cooling (dark blue). (b) Normalized $\rho(T)$ of sample B4 for several $\mu_0 H \leq 15$ T. Increasing H indicated by an arrow at high temperatures; note that the maximum value of the resistivity at low T decreases with increasing H . Inset: low- T behavior of $\rho(T)$ between 2.5 and 6 T. The emerging maximum is marked by up arrows for $\mu_0 H \geq 2.5$ T. The SDW transition is shown by down arrows. (c) Resistivity of sample B1 for $15 \leq \mu_0 H \leq 30$ T. Curves are offset for clarity. Black arrows at low T mark the inflection point for $\mu_0 H > 15$ T. Inset: minimum in ρ ; arrows track the suppression of T_{\min} with increasing H .

92 mJ mol⁻¹ K⁻²) semimetallic \mathcal{L} -phase [9, 15–17] to the \mathcal{H} -phase, characterized by a simple, almost spherical Fermi surface with a light effective mass [1]. Band structure calculations for the \mathcal{L} -phase confirm the gapless ground state and predict the system to become a topological semimetal or topological Kondo insulator under applied strain [16, 17]. In Ref. [1], an attempt to trace the high-temperature limits of the $\mathcal{L} - \mathcal{H}$ boundary was made using $\chi = \partial M / \partial H$ contours, where M is the magnetization; however, subsequent experiments suggested that χ was not an accurate indicator of the (H, T) position of the valence transition, prompting the current comprehensive series of measurements that reveal the much more unusual behavior shown in Fig. 1.

CeOs₄Sb₁₂ single crystals were prepared using a molten-flux technique [15] with an excess of Sb. Further details can be found in [1]. Several single crystals (cubic space group T_h^5 ($Im\bar{3}$), no. 204) were obtained from the same growth batch. Four bar-shaped crystals (samples B1–B4) were used to measure resistivity with the standard four-probe techniques with the current applied along the [100] direction.

Magnetic fields of up to 15 T (30 T) were provided by superconducting (water-cooled resistive) magnets. A Proximity-Detector-Oscillator (PDO) technique was used for contactless (MHz) measurements of the resistivity in pulsed magnetic fields. Shifts in the PDO frequency f are caused by alterations in the sample skin depth [18, 19], leading to $\Delta f \propto -\Delta\rho$ for small relative changes in ρ [18]. Magnetostriction was measured by the Fiber Bragg Grating technique [20], also in pulsed mag-

netic fields. The magnetic field was applied along the [100] direction for all measurements.

Fig. 2(a) shows $\rho(T)$ for crystals B1–B4 at $H = 0$. In agreement with previous studies [9, 15], the $H = 0$ resistivity initially decreases upon cooling, reaching a minimum at $T = T_{\min}$. Below this, $\rho(T)$ increases quasi-logarithmically. The minimum in ρ has previously been interpreted as the $\mathcal{H} - \mathcal{L}$ transition [1]. However, in contrast to that earlier work, the current study shows that the exact value of T_{\min} at $H = 0$ is strongly sample-dependent, ranging from 17.5 K to 48.5 K for the crystals studied. Similar sample-dependent variations in the low-temperature magnetic and transport properties of other Ce-based skutterudites were observed previously [21, 22], and have been attributed to a delicate balance between competing scattering effects and the influence of magnetic impurities.

Note also that there is a small but consistent hysteresis between cooling and warming for the position of the ρ minimum, with T_{\min} being higher on cooling than on warming [inset of Fig. 2(a)]. The difference increases with T -sweep rate, but is never less than 0.5 K for the slowest sweeps. Similar hysteretic behavior in both ρ and χ has been observed close to the valence transitions in YbInCu₄ [23], Ce [2] and cerium alloys [3], supporting the proposal [1] that the valence of Ce in CeOs₄Sb₁₂ changes at the $\rho(T)$ minimum.

The shape of the $\rho(T)$ curves changes significantly when magnetic field is applied. Fig. 2(b) shows normalized resistivity curves $\rho(T)/\rho(300\text{ K})$ for sample B4 for several fields up to 15 T. Increasing H initially shifts the

position of the minimum to higher T ; subsequently, T_{\min} is almost field independent between 3 and 15 T, but then decreases [inset to Fig. 2 (c)].

Antiferromagnetic order, believed to be due to spin-density wave (SDW) formation, has been observed in $\text{CeOs}_4\text{Sb}_{12}$ below 1 K at $H = 0$ [8, 24, 25]; the transition temperature, T_{SDW} , was seen to increase with H to 2 K at 7 T and subsequently decrease [1, 9, 10]. Following similar data in earlier measurements [9], we attribute the kink in our $\rho(T)$ curve [marked by down arrows; inset of Fig. 2 (b)] to the transition to the SDW. The behavior of T_{SDW} in our data accords with earlier work [9].

For fields higher than 3 T, a local maximum in $\rho(T)$ develops at a temperature T_{\max} just above T_{SDW} (up arrows in the inset) and shifts to higher T with increasing H . No hysteresis was observed in the position of either the maximum or the SDW transition. T_{\max} shows an almost linear field dependence; in addition, as H grows, the maximum in $\rho(T)$ becomes broader and lower. These trends continue for fields of up to 30 T, as shown in Fig. 2 (c).

As will be clear from Fig. 1, for $\mu_0 H > 10$ T, it is possible for a constant H T -sweep to traverse the valence transition twice: $\mathcal{H} - \mathcal{L}$, followed by $\mathcal{L} - \mathcal{H}$. In this context, the maximum in $\rho(T)$ at T_{\max} is a precursor to the restoration of metallic behavior at low T . For $\mu_0 H \geq 10$ T, we find an inflection point in $\rho(T)$ at $T = T_{\text{inff}}$, which we attribute to the valence transition; below this, metallic resistivity $\rho(T) = \rho_0 + AT^2$ is obeyed. T_{inff} is marked by down arrows in Fig. 2 (c) and indicated by solid squares in the phase diagram in Fig. 1. For fields between 3.5 T, where the maximum in $\rho(T)$ first emerges, and 11 T, the SDW phase interposes itself and T_{inff} is not visible. Nevertheless, within the region between T_{\max} and T_{SDW} , $\text{CeOs}_4\text{Sb}_{12}$ begins to revert to metallic behavior (*i.e.*, $\rho(T)$ falls as T decreases).

The high- H , low- T part of the $\mathcal{L} - \mathcal{H}$ phase boundary that partially coincides with the suppression of the SDW phase was initially identified using PDO experiments for $T \leq 4$ K [1]; in the current work, we use the same technique to track the transition to higher T . Fig. 3 (a) shows the change in PDO frequency in $\text{CeOs}_4\text{Sb}_{12}$ in fields of up to 60 T for several T between 0.7 and 40 K. For low T there is a pronounced maximum at low fields, followed by a sharp decrease of $-\Delta f$ and a minimum at high fields. Since $-\Delta f$ is proportional to $\Delta\rho$, we can analyse the PDO $-\Delta f$ data in an analogous way to the $\rho(T)$ data. The maxima in both properties have the same field dependence, and the PDO maximum continues to move linearly to higher fields with increasing T . As in the $\rho(T)$ data, the maximum is the precursor of a change from semimetallic behavior (\mathcal{L} phase) to metallic character (\mathcal{H} phase). The succeeding drop in ρ (or $-\Delta f$) is commensurate with removing Ce f -electrons from the \mathcal{L} -semimetallic ground state with its ultra-heavy effective masses, the resulting shift in Fermi energy producing the much larger, almost-spherical Fermi surface (with

light-mass quasiparticles) of the \mathcal{H} -phase predicted by theory and observed in experiment [1, 16, 17]. As in Ref. [1], we identify the $\mathcal{L} - \mathcal{H}$ transition as the inflection point within the fall in $-\Delta f$; this is shown as arrows in Fig. 3 (a). Hysteresis occurs between PDO data recorded with rising and falling H , again suggestive of the lossy kinetics typical of valence transitions [3].

Changes in sample volume frequently accompany valence transitions [2–4]; therefore pulsed-field magnetostriction measurements were carried out for $0 \leq \mu_0 H \leq 60$ T and $0.5 \leq T \leq 40$ K. Typical results are shown in Fig. 3 (b) as fractional change in length ($\Delta L/L$) versus H . The $\mathcal{L} - \mathcal{H}$ phase transition is marked by a change of slope: the initial decrease of $\Delta L/L$ slows down and is reversed or becomes flat, causing an elbow in the data.

Linear functions are fitted to the data below and above the elbow; the transition field is then defined as the point at which the gradient of the data is equal to the mean of the gradients of the two linear functions. Examples of linear fits for 0.55 and 12 K are shown. The resulting transition fields are indicated by arrows in the graph. At low T , the valence transition follows the established border of the SDW to lower H as T increases. Above 4 K this trend reverses; the transition field starts to grow with T . The elbow can be followed up to 22 K; at higher T , it is too weak to be identified reliably.

Shubnikov-de Haas oscillations in $-\Delta f$ occur in the lower- T curves in Fig. 3 (a) above 25 T. These comprise a single frequency $F \approx 1600$ T, due to the roughly spherical Fermi surface [1] of the \mathcal{H} -phase. Using an analysis similar to that in Ref. 27, the quasiparticle effective mass (m^*) was found to be H -dependent. Fig. 3 (c) shows the oscillating part of $-\Delta f$ [right axis] and the development of m^* for several mean fields B_m separated by 0.75 T steps [27]. The Fourier window for this procedure is $\Delta = 1/467 \text{ T}^{-1}$, corresponding to ≈ 3.5 oscillations. At first, m_{eff} increases only slowly with decreasing H , from 3.6 to 4.4 m_e between 56 and 35 T. As the intersection of the \mathcal{L} , \mathcal{H} and SDW phases at lower H approaches, m_{eff} increases more rapidly, reaching 6 m_e at 28.5 T, the lowest field at which a value could be determined.

The above PDO, magnetostriction and transport data (T_{\min} , T_{\max} and T_{inff}) for all four crystals are shown in Fig. 1; the boundaries of the SDW phase have been taken from Refs. [8–11]. It is immediately obvious that the “wedge-shaped” phase boundary surrounding the \mathcal{L} phase is very unusual indeed. Firstly, as mentioned above, the position of the $\mathcal{H} - \mathcal{L}$ transition at T_{\min} differs for the four different samples, ranging from 17.5 to 48.5 K at $H = 0$. Secondly, with increasing H in the range $0 \leq \mu_0 H \leq 2$ T, the transition at first moves rapidly to higher T (*i.e.*, has a positive gradient); amongst the different samples, the difference between the T_{\min} values becomes smaller, but remains at least 4 K up to 30 T. The transition temperature hardly changes between 2 and 15 T but eventually starts to decrease in higher fields.

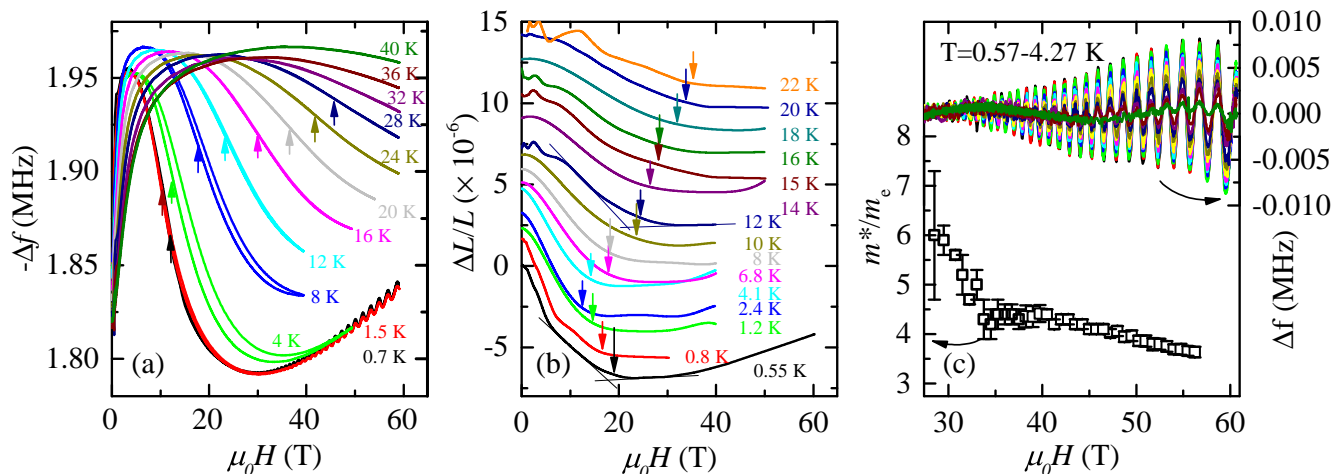


FIG. 3. (a) PDO frequency change $-\Delta f$ in pulsed fields. Note the hysteresis between up and down sweeps. (b) Pulsed-field magnetostriction $\Delta L/L$. Data are offset for clarity. Linear fits are explained in the text. Arrows mark the valence transition in (a) and (b). (c) Oscillatory part of $-\Delta f$ for $0.57 \leq T \leq 4.3$ K, and H -dependence of the effective mass of the $F = 1.6$ kT Shubnikov-de Haas oscillations; here m_e is the bare electron mass.

The metallic \mathcal{H} phase is restored at high H and low T . The field-induced $\mathcal{L} - \mathcal{H}$ transition and destruction of the SDW phase coincide below $T \approx 2$ K and above 10 T. A simple interpretation of this is that the formation of the SDW will be dependent on details of the topology of the \mathcal{L} -phase Fermi surface [29]; once the \mathcal{L} -phase is removed by the valence transition, the SDW will inevitably be destroyed. However, we will see below that the death of the SDW and the $\mathcal{L} - \mathcal{H}$ phase boundary are, chicken-and-egg-like, much more subtly entwined than in this simple interpretation. Whereas the low- T part of the high-field phase boundary has a (relatively conventional) negative gradient, above $T = 2$ K, the phase boundary assumes a positive gradient; the $\mathcal{L} - \mathcal{H}$ transition moves toward higher H with increasing T , showing an almost linear H, T relationship up to 28 K as shown in Fig. 1 and its top inset.

The features that indicate the $\mathcal{H} - \mathcal{L}$ and the precursor to the $\mathcal{L} - \mathcal{H}$ transition in $\rho(T)$ (the local minimum and maximum) move closer together for increasing H , resulting in an almost plateau-like feature at 30 T. This convergence shows that the T -range for which the \mathcal{L} -phase is stable becomes smaller with increasing H . Extrapolating the measured points suggests that above ≈ 55 T, \mathcal{H} should be the only stable phase of $\text{CeOs}_4\text{Sb}_{12}$. A logarithmic scaling of the phase diagram [top inset of Fig. 1] displays this behavior more clearly [26].

The $\mathcal{L} - \mathcal{H}$ phase boundary is clearly very different from most others encountered in condensed-matter physics; unlike *e.g.*, a mean-field boundary [28] or the “domes” observed in many correlated-electron systems such as organic, high- T_c and pnictide superconductors [29–32], the gradient of the boundary in T, H space does not change monotonically, but alternates *positive, negative, positive, negative*. By the same token, it clearly deviates from the *elliptic* ($H^2 \propto T^2$) behavior ex-

pected for the field-induced valence transitions in other cerium based systems [2, 3] or uranium compounds [5].

The elliptic phase boundary usually associated with valence transitions is driven by the T - and H dependences of the free energy of the quasi-localized f multiplet [4]. The energies of the Fermi liquids of the phases on either side of the phase boundary will depend only slightly on H and T , so that the multiplet’s free energy dominates the situation and drives the valence transition. The $-TS$ (where S is entropy) term in the free energy means that the phase in which the multiplet is populated will always be the groundstate at high T and high H [3, 4], the multiplet’s simple partition function resulting in the $H^2 \propto T^2$ elliptic phase boundary [4]. The deviation of $\text{CeOs}_4\text{Sb}_{12}$ from this simple behavior implies that one or more additional energy scales that depend strongly on H and/or T are present.

Turning first to the low- T , high- H portion of the valence transition, recall that the \mathcal{H} -phase quasiparticle effective mass appears to be diverging as the $\mathcal{H} - \mathcal{L}$ transition approaches (Fig. 3). The antiferromagnetic skutterudite $\text{PrOs}_4\text{As}_{12}$ shows a similar mass increase on approaching the phase boundary with its magnetic groundstate [33]. Such effective-mass increases are frequently associated with proximity to a quantum-critical point (QCP) [30, 31, 33]. In the case of $\text{CeOs}_4\text{Sb}_{12}$, the QCP is most likely associated with the field-driven collapse of the SDW (see Fig. 1). The presence of strong quantum fluctuations - probably antiferromagnetic - around the QCP will greatly perturb the free energy of the Fermi liquids on either side of the $\mathcal{L} - \mathcal{H}$ boundary [35], challenging the dominance of the multiplet’s $-TS$ contribution to the free energy [4] as $T \rightarrow 0$.

Moving to the high- T , $H \rightarrow 0$ portion of the $\mathcal{L} - \mathcal{H}$ transition, the most striking feature is the initial, large, positive gradient. Qualitatively similar behavior is seen

in the phase diagram of a reduced-dimensionality anti-ferromagnet [34]; in that case, the effect is attributed to the effect of thermal fluctuations on the free energy of the system. However, the phase-boundary gradient reversal measured in Ref. 34 is much less marked than that in $\text{CeOs}_4\text{Sb}_{12}$ (Fig. 1). Moreover, there is no obvious reason why the mechanism of Ref. [34] would yield the strong sample dependence seen here.

The \mathcal{L} phase of $\text{CeOs}_4\text{Sb}_{12}$ is thought to be highly unusual among Ce compounds in that a very small application of uniaxial stress can transform it into an unusual topological semimetal [17]. It is therefore possible that the inclusions (fraction of a % level) of elemental Ce or Os, in otherwise very high quality $\text{CeOs}_4\text{Sb}_{12}$ crystals, as recently observed in neutron scattering experiments [36] result in local regions of varying uniaxial stress that induce topologically-protected “domains”. The number of these domains would likely be very dependent on sample quality, and even small variations in strain within the same batch could give rise to the observed sample dependence. In addition, the band structure associated with such states can be very sensitively dependent on magnetic field (see *e.g.* Refs. [27, 37] and citations therein) perhaps leading to the initial positive gradient of the \mathcal{L} - \mathcal{H} boundary. Experimentally, the presence of even a small fraction of similar quasiparticles in an otherwise unremarkable Fermi liquid can have a disproportionate effect on measurable macroscopic properties [27]. Analogous effects may well be being manifested in the unusual low- H , high- T curvature of the $\text{CeOs}_4\text{Sb}_{12}$ valence transition.

In summary, the H - T -phase diagram of $\text{CeOs}_4\text{Sb}_{12}$ has been mapped using resistivity, magnetostriction, and MHz conductivity. The \mathcal{L} and the \mathcal{H} phase are separated by a valence transition that exhibits a wedge-shaped phase boundary. This behavior is clearly distinct from the text-book “elliptical” phase boundary usually followed by valence transitions. Field-dependent effective masses have been revealed by Shubnikov-de Haas oscillations within the \mathcal{H} phase showing an increasing m^* as H drops toward the \mathcal{H} - \mathcal{L} phase boundary, suggesting proximity to a QCP. The associated magnetic fluctuations may be responsible for the anomalous H, T dependence of the valence transition at high H . The unusual low- H , high- T portion of the phase boundary may in contrast be associated with the proximity of $\text{CeOs}_4\text{Sb}_{12}$ to a topological semimetal induced by uniaxial stress, resulting in strongly sample-dependent behavior.

We thank Roger Johnson for constructive discussions. Research at CSU-Fresno is supported by NSF DMR-1506677; at UCSD by NSF DMR-1206553 and US DOE DEFG02-04ER46105; at Hokkaido University by JSPS KAKENHI JP15KK0146, JP18H04297, JP17K05525; at University of Warwick by the EPSRC and European Research Council (ERC) under the European Unions Horizon 2020 research and innovation programme (grant agreement No 681260). Work performed at the National

High Magnetic Field Laboratory, USA, was supported by NSF Cooperative Agreements DMR-1157490 and DMR-1644779, the State of Florida, U.S. DoE, and through the DoE Basic Energy Science Field Work Project Science in 100 T. We acknowledge the support of the HFML-RU/FOM, member of the European Magnetic Field Laboratory (EMFL).

-
- [1] P. C. Ho, J. Singleton, P. A. Goddard, F. F. Balakirev, S. Chikara, T. Yanagisawa, M. B. Maple, D. B. Shrekenhamer, X. Lee, and A. T. Thomas, *Phys. Rev. B* **94**, 205140 (2016).
 - [2] D. C. Koskenmaki and K. A. Gschneider, *Handbook on the Physics and Chemistry of Rare Earths*, Vol. 1 (edited by K. A. Gschneider and L. Eyring (North Holland, Amsterdam), 1978) p. 337 ff.
 - [3] F. Drymiotis, J. Singleton, N. Harrison, J. C. Lashley, A. Bangura, C. H. Mielke, L. Balicas, Z. Fisk, A. Migliori, and J. L. Smith, *J. Phys. Condens. Matter* **17**, L77 (2005).
 - [4] M. O. Dzero, L. P. Gorkov, and A. K. Zvezdin, *J. Phys. Condens. Matter* **12** L711 (2000).
 - [5] N. Harrison and M. Jaime, arXiv:1902.06588 [cond-mat.str-el] (2019).
 - [6] J. C. Lashley, J. Singleton, A. Migliori, J. B. Betts, R. A. Fisher, J. L. Smith, and R. J. McQueeney, *Phys. Rev. Lett.* **91**, 205901 (2003).
 - [7] N. Harrison, J. B. Betts, M. R. Wartenbe, F. F. Balakirev, S. Richmond, M. Jaime, and P. H. Tobash, arXiv:1902.06859 [cond-mat.str-el] (2019).
 - [8] T. Namiki, Y. Aoki, H. Sugawara, and H. Sato, *Acta Physica Polonica B* **34**, 1161 (2003).
 - [9] H. Sugawara, S. Osaki, M. Kobayashi, T. Namiki, S. R. Saha, Y. Aoki, and H. Sato, *Phys. Rev. B* **71**, 125127 (2005).
 - [10] C. R. Rotundu and B. Andraka, *Phys. Rev. B* **73**, 144429 (2006).
 - [11] T. Tayama, W. Ohmachi, M. Wansawa, D. Yutani, T. Sakakibara, H. Sugawara, and H. Sato, *J. Phys. Soc. Jpn.* **84**, 104701 (2015).
 - [12] E. D. Bauer, N. A. Frederick, P.-C. Ho, V. S. Zapf, and M. B. Maple, *Phys. Rev. B* **65**, 100506 (2002).
 - [13] M. B. Maple, P.-C. Ho, V. S. Zapf, N. A. Frederick, E. D. Bauer, W. M. Yuhasz, F. M. Woodward, and J. W. Lynn, *J. Phys. Soc. Jpn.* **71**, 23 (2002).
 - [14] P.-C. Ho, W. M. Yuhasz, N. P. Butch, N. A. Frederick, T. A. Sayles, J. R. Jeffries, M. B. Maple, J. B. Betts, A. H. Lacerda, P. Rogl *et al.* *Phys. Rev. B* **72**, 094410 (2005).
 - [15] E. D. Bauer, A. Slebarski, E. J. Freeman, C. Sirvent, and M. B. Maple, *J. Phys. Condens. Matter* **13**, 4495 (2001).
 - [16] H. Harima and K. Takegahara, *J. Phys. Condens. Matter* **15**, S2081 (2003).
 - [17] B. Yan, L. Muehler, X.-L. Qi, S.-C. Zhang, and C. Felser, *Phys. Rev. B* **85**, 165125 (2012).
 - [18] S. Ghannadzadeh, M. Coak, I. Franke, P. A. Goddard, J. Singleton, and J. L. Manson, *Rev. Sci. Instrum.* **82**, 113902 (2011).
 - [19] M. M. Altarawneh, C. H. Mielke, and J. S. Brooks, *Rev.*

- Sci. Instrum. **80**, 066104 (2009).
- [20] M. Jaime, C. Corvalán Moya, F. Weickert, V. Zapf, F. F. Balakirev, M. Wartenbe, P. F. S. Rosa, J. B. Betts, G. Rodriguez, S. A. Crooker *et al.* *Sensors* **17**, 2572 (2017).
- [21] G. P. Meisner, M. S. Torikachvili, K. N. Yang, M. B. Maple, and R. P. Guertin, *J. Appl. Phys.* **57**, 3073 (1985).
- [22] E. D. Bauer, A. Slebarski, R. P. Dickey, E. J. Freeman, C. Sirvent, V. S. Zapf, N. R. Dilley, and M. B. Maple, *J. Phys. Condens. Matter* **13**, 5183 (2001).
- [23] C. D. Immer, J. L. Sarrao, Z. Fisk, A. Lacerda, C. Mielke, and J. D. Thompson, *Phys. Rev. B* **56**, 71 (1997).
- [24] M. Yogi, H. Kotegawa, G.-q. Zheng, Y. Kitaoka, S. Ohsaki, H. Sugawara, and H. Sato, *J. Phys. Soc. Jpn.* **74**, 1950 (2005).
- [25] C. Yang, Z. Zhou, H. Wang, J. Hu, K. Iwasa, H. Sugawara, and H. Sato, *Rare Metals* **25**, 550 (2006).
- [26] Note that the $\mathcal{L} - \mathcal{H}$ transition becomes very difficult to observe in the pulsed-field PDO data above 28 K, as it moves toward merging with the high- T part of the phase boundary close to 40 K. As the upper part of the boundary is very flat in the T, H plot, it is challenging to resolve in any swept-field, constant- T pulsed experiment; the corresponding feature in the data will be very broad. Following the flatter, upper boundary to higher fields would be best accomplished using swept- T , fixed- H PDO measurements, but, as with the ρ data, sadly, these would be limited to $\mu_0 H \leq 30$ T by the resistive magnet used.
- [27] D. J. Rebar, S. M. Birnbaum, J. Singleton, M. Khan, J. C. Ball, P. W. Adams, J. Y. Chan, D. P. Young, D. A. Browne, and J. F. DiTusa, *Phys. Rev. B* **99** 094517 (2019).
- [28] P.M. Chaikin, and T.C. Lubensky, *Principles of condensed matter physics* (4th print ed.), Cambridge: Cambridge University Press (2007)
- [29] J. Singleton, *Reports on Progress in Physics* **63** 1111 (2000).
- [30] B.J. Ramshaw, S. E. Sebastian, R. D. McDonald, James Day, B. S. Tan, Z. Zhu, J. B. Betts, Ruixing Liang, D. A. Bonn, W. N. Hardy *et al.*, *Science* **348** 317 (2015).
- [31] B. Michon, C. Girod, S. Badoux, J. Kačmarčík, Q. Ma, M. Dragomir, H. A. Dabkowska, B. D. Gaulin, J.-S. Zhou, S. Pyon *et al.*, *Nature* **567** 218 (2019).
- [32] Q. Si, R. Yu and E. Abrahams, *Nature Reviews Materials* **1** 16017 (2016)
- [33] P.-C. Ho, J. Singleton, M. B. Maple, H. Harima, P. A. Goddard, Z. Henkie, and A. Pietraszko, *New J. Phys.* **9**, 269 (2007).
- [34] P. Sengupta, C. D. Batista, R. D. Mc Donald, S. Cox, J. Singleton, L. Huang, T. P. Papageorgiou, O. Ignatchik, T. Hermannsdörfer, J. L. Manson *et al.*, *Phys. Rev. B* **79**, 060409 (2009).
- [35] The strong perturbation of the Fermi-liquid free energy is visibly manifested in the field-dependent renormalization of the effective mass.
- [36] M. J. Pearce *et al.*, in preparation.
- [37] P. Tang, Q. Zhou, and S.-C. Zhang, *Phys. Rev. Lett.* **119**, 206402 (2017).